Structure of the Catalytic Active Sites in Vanadium-Doped Aluminophosphate Microporous Materials. New Evidence from Spin Density Studies

(Article begins on next page)

18 October 2024

Structure of the Catalytic Active Sites in Vanadium Doped Alumino Phosphate Microporous Materials. New Evidence from Spin Density Studies.

Sara Maurelli,[1] Gloria Berlier,[1] Mario Chiesa*[1] Federico Musso,[2] Furio Corà [2]

[1]Dipartimento di Chimica, Università di Torino and NIS Centre, via P. Giuria 7, 10125, Torino,

Italy

[2] Department of Chemistry, University College London, 20 Gordon Street, London WC1H 0AJ, UK

*Corresponding Author: e-mail: mario.chiesa@unito.it

Abstract

Electron spin resonance and hyperfine sublevel correlation (HYSCORE) spectroscopy at X- and Q-band frequencies have been employed, in conjunction with DFT modelling, to determine the location of V(IV) ions in AlPO-5 zeotype materials. Two EPR active species are detected, whose spin Hamiltonian parameters are in accord with vanadyl ions (VO^{2+}) experiencing slightly different local environments. Interactions of the unpaired electrons of the paramagnetic VO^{2+} species with all relevant nuclei (^1H, ^{31}P, ^{27}Al and ^{51}V) could be resolved allowing for the first detailed structural analysis of the VO^{2+} paramagnetic ions in AlPO materials. Dehydration treatments indicate that the observed ^1H hyperfine couplings stem from structural protons in the first coordination sphere of the VO^{2+} species, strongly pointing to charge compensating mechanisms associated to isomorphous framework substitution at Al^{3+} sites, in good agreement with the large ^{31}P hyperfine couplings. Detection of fairly large ^{27}Al couplings point to the presence of VO^{2+}-O-Al linkages associated to a different structural arrangement, in agreement with the presence of two EPR active species. The interpretation of the experimental results is corroborated by DFT modelling, which affords a microscopic description of the system investigated. The two EPR active species are found to be consistent with isolated VO^{2+} species isomorphously substituted in the AlPO framework at Al^{3+} sites and extra-framework VO^{2+} species docked in the center of the 6 membered rings that line up the main channel of the AFI structure.

2

Introduction

Microporous aluminophosphates (AlPOs), when activated via the inclusion of dopant ions in the framework, have widespread applications in the field of heterogeneous catalysis.[1-3] AlPOs are zeolite-like materials in which silicon ions are replaced by phosphorus and aluminum in strict alternation, forming a 3-dimensional neutral oxide network that can adopt a range of polymorphic structures.[4] In these materials, Al and P ions can be isomorphically replaced by di-, tri-, and tetra-valent heteroatoms in a relatively easy and controllable manner, giving rise to acid, redox, and even bifunctional properties.[5] Of particular importance for oxidation reactions are the so-called MeAPO materials in which Al ions are replaced by redox-active transition metals, such as Co, Mn, Fe, Cr etc.[6-10] These materials combine the reactivity of the redox-active cations with high surface area and the unique spatial constraints imposed by the molecular dimensions of their porous network.[11-13]

The structure and reactivity of divalent heteroatoms in MeAPOs has been thoroughly investigated, particularly for Co and Mn doped materials.[3] It is well known that these divalent ions usually substitute for trivalent Al framework atoms as tetrahedral sites, resulting in a Brönsted functionality (necessary to compensate the negative charge delocalized on the framework) which disappears after a reversible oxidation to the trivalent state.[10,14-18] More complex is the situation when tetravalent ions are inserted in the AlPOs framework, as in the case of Ti^{4+} or V^{4+} ions. Simple chemical considerations would suggest the idea that both ions are substituting for pentavalent P atoms, generating a negative charge on the framework stabilized by a Al(OH)Me Brönsted site.[19-23] However, recent work from some of us gave clear-cut evidence for the presence of reducible Ti ions at Al sites in TiAPO-5, suggesting that the framework neutrality can be obtained by replacement of Al and P couples by two Ti ions.[24,25] to form Me^{4+} clusters reminiscent of the Si islands in SAPOs.

VAPOs are size and shape selective oxidation catalysts[22,26,27] that are exploited in processes including alkane ammoxidation and alkene epoxidation.[28-30] These selective oxidation catalysts have also been shown to exhibit a high degree of selectivity with yields in excess of 95% in oxidative dehydrogenation, for example in the conversion of propane to propene.[13,31,32] VAPOs can also exhibit bi-functional catalysis when combined with other dopant ions, such as Si or Ti, making them quite remarkable catalysts.[22,26,33,34]

The structure of V ions in AlPOs frameworks is still the subject of an open debate,[35] due to the complex chemistry and coordinative flexibility of the oxovanadium species, (V^{4+}=O or V^{5+}=O vanadyls), being the vanadyl ion the usual source of vanadium in the VAPO synthesis.[19,20,36,37] A

3

major source of complexity associated with studying VAPOs is the vanadium ion's ability not only to adopt different oxidation states, but also to occupy both framework and extraframework positions. Furthermore, V ions in solution can give rise to oligomerisation and yield polynuclear clusters. Finally, depending on the synthesis conditions, vanadium may adopt different coordination numbers.[38] The combination of these factors makes the characterisation of V in AlPO, and hence "mapping" its behaviour, a difficult task for both experimental and computational studies.[39]

In this work, the structure of V ions in VAPO-5 is investigated by means of a combination of multi-frequency Continuous Wave (CW) and Pulse Electron Paramagnetic resonance (EPR) experiments and computational modelling.

EPR is one of the most powerful methods to obtain a detailed description of the local structure of vanadium centers in their +4 (paramagnetic) oxidation state ($3d^1$, $S=1/2$). In particular, so called hyperfine techniques (HYSCORE and ENDOR) have been proven extremely useful to elucidate the local topology of vanadium containing heterogeneous catalysts in general [40-44] and the nature of paramagnetic transition metal ions such as Ti, V and Mn in AlPOs in particular.[24,25,45-47] In the case of AlPOs both aluminum and phosphorous have suitable magnetic properties for the investigation of long range magnetic interactions by high resolution EPR techniques, which allow discriminating between different substitutional sites. In particular in the present work the major spectroscopic information obtained are the ^{1}H, ^{31}P and ^{27}Al ligand hyperfine interactions (*hfi*), which are measured by means of HYSCORE spectroscopy at X- and Q- band frequencies. These magnetic interactions provide direct access to specific binding site and geometry of paramagnetic vanadium species, observed prior and after calcination of the sample. For the analysis of the ligand *hfi* couplings, periodic DFT computations were employed in order to interpret the experimentally obtained data in terms of microscopic model structures for V incorporation in AlPO materials.

2. Materials and Methods

2.1 Materials.

VAPO-5 sample was prepared by hydrothermal synthesis out using triethylamine (minimum 99%) as structure-directing agents (SDA), aluminium isopropoxide (98+%), phosphoric acid (≥85 wt.%), vanadyl sulfate hydrate (97%) and deionized water. All reactants were purchased from Sigma-Aldrich and were employed as received. The synthesis was carried out as described in Ref. 35. After the synthesis, the product was calcined by heating gradually in a nitrogen flow and leaving the samples in an oxygen flow at 873 K for 12 hours. The sample formula $Al_{16.1}P_{16.9}V_{0.2}O_{66.3}$ was calculated by EDX analysis, corresponding to a V loading of 0.58 wt%.[35]

4

The calcined sample was dehydrated at 423K for one hour under high vacuum pumping. The reduction treatment was carried out in hydrogen atmosphere (100 mbar) at T = 673K for two hours.

2.2 Spectroscopic methods.

X-band CW EPR spectra were detected at 77K on a Bruker EMX spectrometer (microwave frequency 9.75 GHz) equipped with a cylindrical cavity. A microwave power of 10 mW, modulation amplitude of 0.15 mT and a modulation frequency of 100 KHz were used.

Pulse EPR experiments at X-band (9.76 GHz) and Q-band (34 GHz) were performed on an ELEXYS 580 Bruker spectrometer equipped with a liquid-helium cryostat from Oxford Inc. The magnetic field was measured by means of a Bruker ER035M NMR gauss meter.

Electron-spin-echo (ESE) *detected EPR*. The experiments were carried out with the pulse sequence: $\pi/2 - \tau - \pi - \tau - echo$. At X-band, the mw pulse lengths $t_{\pi/2} = 16$ ns and $t_\pi = 32$ ns and a τ value of 200 ns were used. Q-band conditions were as follows: $t_{\pi/2} = 16$ ns and $t_\pi = 32$ ns and a τ value of 400 ns. Further experimental details are specified in the figures caption. A 1 kHz repetition rate was used at both X- and Q- band frequencies

Hyperfine Sublevel Correlation (HYSCORE) [48] experiments were carried out with the pulse sequence $\pi/2 - \tau - \pi/2 - t_1 - \pi - t_2 - \pi/2 - \tau - echo$. At X-band the parameters were: mw pulses of lengths $t_{\pi/2} = t_\pi = 16$ ns, starting times 96 ns for t_1 and t_2, $\Delta t = 8$ ns (data matrix 350 × 350). Spectra with different τ values (96 ns 136 ns and 250 ns) were recorded at T=20 K. At Q-band the following parameters were used: mw pulses of lengths $t_{\pi/2} = 16$ ns, $t_\pi = 24$ ns, starting times 200 ns for t_1 and t_2, and time increments $\Delta t = 8$ ns (data matrix 350 × 350). Spectra with different τ values, specified in the figures caption, were recorded at T = 35 K. A shot repetition rate of 1.25 kHz was used at both X- and Q- band frequencies. A four-step phase cycle was used to remove unwanted echoes. The time traces of the HYSCORE spectra were baseline corrected with a third-order polynomial, apodized with a Hamming window and zero filled. After two-dimensional Fourier transformation, the absolute value spectra were calculated. The spectra were added for the different τ values in order to eliminate blind-spot effects.

EPR and HYSCORE spectra were simulated using the Easyspin package.[49] The errors in the determination of the spin-Hamiltonian parameters were obtained by visual inspection of simulated and experimental spectra.

2.3 Computational methods.

5

The VAPO-5 materials have been simulated using periodic models that are more suitable than molecular fragments to represent the extended crystalline environment of the V ions.[50] The periodic DFT calculations were performed using the CRYSTAL software package.[51,52] Two structures representative of monomeric V centers in the AlPO-5 framework, and compatible with the experimental findings, were investigated. We performed a full structure optimization at the B3LYP [53,54] level of theory.

The wave function of the systems is described as a linear combination of atomic orbitals expressed as a contraction of Gaussian-type functions. A triple-valence plus polarization basis set for V, a double-valence plus polarization basis set for P, Al and O, and a single-valence plus polarization basis set for H have been used. All basis set are available on the online library of the CRYSTAL code.[55] Internal coordinates and lattice vectors have been optimized for each structure with no symmetry constraint in P1 space group, in order to ensure a full relaxation of V and its environment inside the cell.

The periodic DFT study has been complemented with molecular calculations, performed using the ORCA code,[56,57] in order to estimate the **g**-tensor of V that cannot be calculated with CRYSTAL. Two clusters including V and its first coordination sphere have been cut out from the optimized periodic structures obtained with CRYSTAL, as represented in Figure 4. The resulting unsatisfied valences have been saturated with H atoms oriented along the broken bonds. The **g**-tensor has been calculated keeping the atom coordinates fixed, *i.e.* maintaining V and its local environment as in the optimized periodic models, with a Ahlrichs TZVPP basis set.[58]

Since the value of a_{iso} is known to be very sensitive to the exchange functional employed, in particular for transition metal ions, [59] calculations have been repeated with the BHandHLYP [54,60] functional and a_{iso} values are reported for both B3LYP and BHandHLYP functionals.

The EPR hyperfine tensor elements of V, P and Al are in excellent agreement between B3LYP and BHandHLYP, and between CRYSTAL and ORCA calculations, hence only B3LYP periodic results will be discussed here. A more complete computational analysis of VAPO-5 detailing the energetics of the different structures, based on periodic DFT calculations will be the object of a forthcoming paper.

3. Results and discussion.

VAPO-5 samples were characterized by powder X-ray diffraction (PXRD), which confirmed the crystallinity and phase purity prior and after calcination at 823 K. The XRD pattern of the

6

calcined sample is reported in the Supporting Information (Figure S1), together with the pattern measured after repeated oxidation/reduction cycles. Both data matched both in position and intensity with the pattern expected for the AFI structure type. Moreover, no appreciable changes could be observed after the redox treatments, confirming the stability of the structure upon changes in the oxidation state of the vanadium heteroatom. The Diffuse Reflectance (DR) UV-Vis spectra of the material were discussed in Ref. 35, with particular attention to the changes induced by redox treatments. In this context, it is sufficient to recall that the presence of $V^{4+}=O$ (vanadyl)species was inferred by the presence of relatively intense and broad bands related to the corresponding ligand field d-d transitions, which closely resembled those reported for the oxovanadiumv (IV) $[VO(H_2O)_5]^{2+}$ ions.[61]

3.1 EPR Experiments.

The X- and Q- band EPR spectra of the as-synthesized VAPO-5 are shown in Figure 1 along with the corresponding computer simulations. The spectra do not change in the temperature interval 10-80 K and are characterized by an eight-fold hyperfine splitting of all anisotropic components typical of V^{4+} (^{51}V I=7/2, abundance 99.76%). The well resolved ^{51}V *hfi* pattern and absence of broad absorption bands suggests a high dispersion of the VO^{2+} species and absence of clustered or polymeric V^{4+} units. Careful inspection of the X-band spectrum reveals that two species with slightly different spin-Hamiltonian parameters contribute to the overall spectral pattern. The spin Hamiltonian parameters of the two species deduced from computer simulation of the X- and Q-band spectra are reported in Table 1 and agree with previous literature data.[19,20,45,62] In Table 1 the signs of the experimental *hfi* tensor elements were chosen such that agreement with the signs of the calculated A values was maintained (*vide infra*) i.e. assuming the sign of the experimental A values to be all negative, in agreement with previous experimental and theoretical work.[40,59] The abundance ratio between the two species was found, based on computer simulation, to be of the order of 1:0.7 in fair agreement with the results of Ref. 45.

An empirical correlation between the g_{iso} (g_{iso}=(g_1+g_2+g_3)/3) and ^{51}V a_{iso} (a_{iso}=(A_1+A_2+A_3)/3) has been proposed, that allows discriminating between VO^{2+} and V^{4+} centers.[63] The EPR parameters reported for tetrahedral V^{4+} species in different matrices are more variable than those of VO^{2+}, however, a correlation between the isotropic spin-Hamiltonian parameters can be empirically exploited to distinguish between the two cases. Indeed, as already emphasized by Ref. 64 the spin Hamiltonian parameters reported in Table 1 are incompatible with V^{4+} species in tetrahedral coordination, indicating that two VO^{2+} species, with slightly different environments are responsible for the observed EPR spectra. This is in accord with what suggested by the adsorption of probe

molecules, monitored by IR spectroscopy that showed the presence of two VO^{2+} ions with similar coordination state but different Lewis acidity. [35]
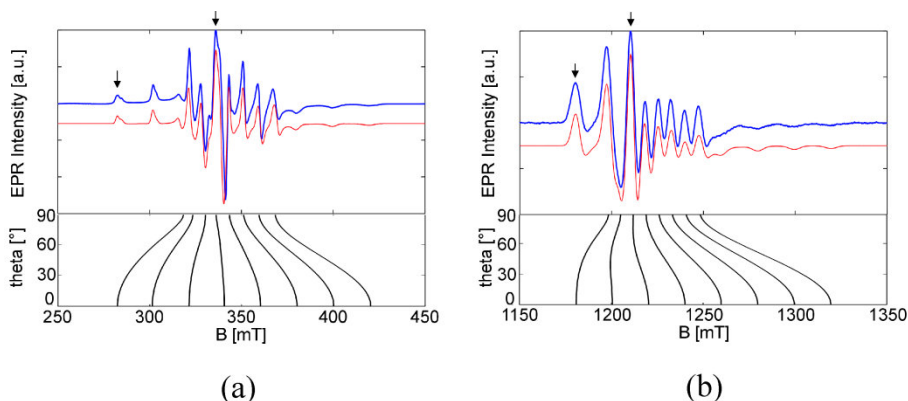

Figure 1. Experimental (blue line) and simulated (red line) EPR spectra of as-synthesized VAPO-5. (a) X- band CW EPR spectrum recorded at 77 K; (b) Q-band ESE detected EPR spectrum recorded at 30 K. To facilitate the comparison with the X-band CW EPR spectrum, the first derivative of the Q-band ESE detected EPR spectrum is presented in (b). The spin-Hamiltonian parameters used to fit both spectra are reported in Table 1.The calculated magnetic resonance fields dependent on the angle θ between the g_3 axis of the V^{4+} **g** tensor and the external magnetic field are shown. The arrows indicate the field positions at which the HYSCORE spectra have been taken.

Analogous spectra were recorded on calcined samples that were dehydrated at 423 K for 1 hour under high vacuum. Under these circumstances a mild reduction of the calcined sample occurs leading to the formation of V^{4+} from previously oxidized (EPR silent) V^{5+} species. This result is at variance with ref.19, where a change in the spectral features upon dehydration of the sample was reported. Reduction of the calcined sample with H_2 at 623K leads to a change in the CW-EPR spectrum (Supporting Information) suggesting a modification of the local coordination geometry of the VO^{2+} centers upon the more severe reducing treatment. Comparison of the field swept EPR spectra obtained upon the different treatments is shown in the Supporting Information section, where the spin-Hamiltonian parameters of the reduced systems are given (Table S1 of Supporting Information). Importantly, the local environment of the VO^{2+} centers as probed by HYSCORE spectroscopy (see the following section) remains unaltered upon high temperature reduction indicating that the variations in the **g** and ^{51}V *hfi* tensors observed in the field swept EPR spectra are due to a structural modification of the site induced by the strong reducing treatment and not to a change in the chemical environment (*i.e.* the location) of the VO^{2+} species. A similar observation was made by Prakash and Kevan on a similar VAPO-5 material reduced under similar conditions.[19] In the following we will thus consider the species observed for the as synthesized and mildly reduced calcined samples as representative of the VO^{2+} species incorporated in AlPO-5 materials.

The spin density distribution over neighboring magnetically active nuclei (hyperfine interaction) is one of the most potent indicators of the local environment experienced by a paramagnetic species. Hyperfine interactions with framework ^{27}Al ($I=5/2$) and ^{31}P ($I=1/2$) yield

8

detailed information on the localization and structural geometry of the incorporated VO^{2+} groups. The investigation was performed at X-and Q-band frequencies using HYSCORE and the findings of such experiments are presented in the following section.

Table 1. Spin-Hamiltonian parameters of VO^{2+} centers in as-synthesized VAPO-5. The parameters are obtained from computer simulation of the field swept EPR spectra reported in Figure 1. The hyperfine coupling constants are expressed in MHz. The signs of the hyperfine tensor elements have been chosen in accordance with the results of the DFT calculations.

	g_1 ±0.01	g_2 ±0.01	g_3 ±0.001	$\|A_1\|$ ±5	$\|A_2\|$ ±5	$\|A_3\|$ ±1	a_{iso}	T_1	T_2	T_3	Ab (%)
Species 1	1.978	1.9734	1.9358	209	183	534	-308.7	+99.7	+125.7	-225.3	58
Species 2	1.978	1.9643	1.9375	207	178	515	-300	+93	+122	-215	42

3.2 HYSCORE experiments

HYSCORE is a two-dimensional experiment where correlation of nuclear frequencies in one electron spin (m_S) manifold to nuclear frequencies in the other manifold is created by means of a strong mixing π pulse. In this way a sub-MHz resolution, comparable to that of NMR spectroscopy, can be achieved, allowing to probe the local environment of paramagnetic centers up to the third coordination shell. The X-band HYSCORE spectra of the as received and calcined VAPO-5 sample recorded at observer position $B_0 = 348.8$ mT are reported in Figure 2(a). This magnetic field setting corresponds to the so-called "powder like position" in that almost all orientations are excited and the spectrum reflects a powder-like situation. Experiments were also carried out at the $g_{\parallel}$, $m_I = -7/2$ observer position (292.1 mT) and are shown in the Supporting Information section. It should be noted that due to the hard micro-wave pulses used in the HYSCORE sequence both species 1 and 2 contribute the spectrum at both field positions.
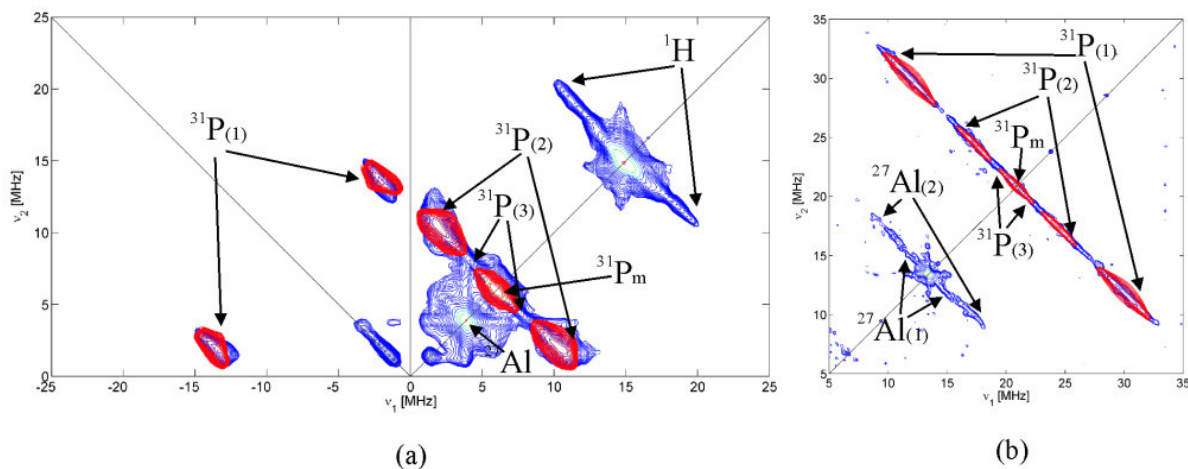
Figure 2. Experimental (blue) and simulated (red) X- band (a) and Q-band (b) HYSCORE spectra of as-synthesized VAPO-5. X-band spectra (a) were recorded at $B_0 = 348.8$ mT and T = 20 K, and spectra recorded at three τ values (96, 136 and 250 ns) are summed together after Fourier transform. Q-band spectra (b) were recorded at $B_0 = 1210.3$ mT and T = 40 K. Spectra recorded at two τ values (184, 260 ns) are summed together after Fourier transform. The ^{31}P

9

hyperfine values used to fit both frequencies are reported in Table 2. The contribution of remote phosphorous nuclei (P_m) is added to the simulation.

The X-band HYSCORE spectrum is characterized by a pronounced ridge, centered at about 15 MHz (the [1]H Larmor frequency at this magnetic field) with a maximum width of about 13 MHz and by peaks from weakly coupled [27]Al and ^{31}P matrix nuclei located on the diagonal of the (+,+) quadrant at the corresponding nuclear Larmor frequencies (Figure 2 (a)). In addition to the diagonal peaks, three pairs of cross features can be distinguished, designated as $P_{(1)}$, $P_{(2)}$, and $P_{(3)}$ in Figure 2a. Cross-peaks $P_{(1)}$ appear along the diagonal of the (-,+) quadrant centered at approximately (-13.4, +1.8) (-1.8 +13.4) MHz, the two coordinates of each point of the cross peaks differing by approximately $2\nu_P$ = 12.03 MHz. These cross peaks are analogous to those recently reported by some of us in the case of Ti^{3+} species in TiAPO-5.[24] Two other cross features are located in the (+,+) quadrant, centered symmetrically around the diagonal point of ν_P = 6.017 MHz. Cross-peaks $P_{(2)}$ have maxima at ca. (10.5, 2.0) (2.0, 10.5) MHz along the diagonal, while cross peak $P_{(3)}$ appears as a narrow ridge with maximum extension of about 3.5 MHz. Given the fact that the ^{31}P couplings span the so called cancellation condition ($A=2\nu_I$) and signals appear across the two quadrants, the interpretation of the spectrum is not straightforward. A more clear spectrum is obtained by performing the HYSCORE experiment at higher magnetic field (Q-band frequency, 33.4 GHz), so that the dominant interaction is the nuclear Zeeman effect ($A<2\nu_I$) and all spectral features appear in the (+,+) quadrant, centered at the [31]P Larmor frequency. The result is shown in Figure 2(b), where the Q-band HYSCORE spectrum recorded at the magnetic field position B_0 = 1210.3 mT is shown. Three series of cross peaks are now clearly distinguished centered symmetrically around ν_P = 20.879 MHz. The hyperfine coupling constants associated to the three series of cross peaks have been obtained by computer simulation of the X- and Q- band HYSCORE spectra taken at different observer positions (see Supporting Information). The simulation of the ^{31}P pattern is shown as a red contour plot superimposed to the experimental spectrum in Figure 2. The simulation was carried out considering a four spin system (S=1/2 and three I=1/2 ^{31}P nuclei) and the same set of spin-Hamiltonian parameters was used to fit both frequencies. The contribution of remote phosphorous nuclei (indicated with P_m in Figure 2) was added for sake of completeness. It should be noted that not only the frequencies but also the relative intensities of the ^{31}P cross peaks are well reproduced at the two frequencies, which allow placing good confidence in the obtained parameters. The spin Hamiltonian parameters used in the simulation are listed in Table 2, where a positive sign was assumed based on the positive ^{31}P nuclear g factor. This choice is in agreement with the DFT computed values (see section 3.3). All three observed ^{31}P couplings are dominated by the Fermi contact interaction and correlate with values observed in the case of the TiAPO-5 system,

10

previously reported by some of us [24] and for vanadyl phosphate molecular complexes.[65-68] The origin of this fairly large isotropic interaction can be rationalized considering a spin density transfer through the directly coordinated oxygen ions via a through-bond mechanism. The isotropic constant is determined mainly by the unpaired spin density in the 3s orbital of the phosphorous atoms and is proportional to the value of a_0 = 10201.44 MHz, which is computed for unit spin density in this orbital.[69] Including a correction for departure of the g value ($g_{iso}[VO^{2+}]$ = 1.960) from the free electron value (g_e = 2.0023) the spin population in the P 3s orbital can be estimated from the following equation:

$$\rho_{P(3s)} = \frac{a_{iso}}{a_0} \cdot \frac{g_e}{g_{iso}} \tag{1}$$

to be of the order of 0.18% , 0.07% and 0.02% for the three detected ^{31}P nuclei. Comparison can be set to the case of framework substituted Ti^{3+} ions in AlPO-5 materials, where similar spin density transfer over ^{31}P nuclei has been observed.[24] As discussed by different Authors [24,47,68] in the case of similar systems, the amount of spin density transfer is expected to depend markedly on bond angle and distance of the fragment V-O-P, making the Fermi contact term a sensitive structural probe. We shall validate this mechanism by means of DFT calculations (*vide infra*).

In addition to the ^{31}P signals previously discussed, both X- and Q- band spectra show a signal centered at (+3.87, +3.87) MHz in the X-band HYSCORE spectrum and at (+13.42, +13.42) MHz in the Q-band spectrum (Figures 2(a) and 2(b), respectively), coinciding with [27]Al Larmor frequencies at the corresponding magnetic fields. The Q band HYSCORE spectrum provides a better resolution and allows resolving two sets of cross peaks with separation of approximately 2 and 8 MHz. The first set of cross peaks was already observed by Ref. 45, while the second one is reported here for the first time and is not detected at X-band frequency. The signals can be satisfactorily reproduced considering two different [27]Al nuclei with a_{iso} = 4.5 MHz and 2 MHz respectively and $|T|$= 2.5 MHz and 1 MHz (Figure 3a). Considering the value of a_0 = 3367.76 MHz for unit spin density on the [27]Al 3s orbital,[69] the corresponding spin density in the Al 3s orbital is ≈ 0.14% and 0.06% respectively, in line with the spin transfer to the [31]P 3s orbitals. The magnitude of the ^{31}P and [27]Al *hfi* coupling parameters and the comparable spin densities at the two atoms suggest that a fraction of the VO^{2+} species coordinate to framework oxygen atoms with both phosphorous and aluminum framework atoms in the second coordination shell. We remark that the intensity ratio between the [27]Al cross and matrix peaks are found to vary from sample to sample suggesting that the presence of V-O-Al linkages is related to the chemical history of the sample. In particular no

11

evidence for the ^{27}Al cross peaks was observed in a bimetallic TiVAPO sample previously studied by some of us. [33,34] These observations can be rationalized considering the presence of two VO^{2+} families (consistent with the presence of two EPR active species) localized at distinct sites, where at least one site is characterized by the presence of ^{27}Al nuclei in the second coordination shell, an architectural feature typical of an extra-framework site. On the other hand the variation in the ^{27}Al signal intensity observed for different samples, suggests that framework substitution at Al^{3+} sites can explain the observed experimental facts *i.e.* the ^{31}P *hfi* couplings and in particular the presence of structurally bound protons necessary for charge compensation at this site.

.

Table 2. ^{31}P, ^{27}Al and ^{1}H hyperfine coupling values of as-synthesized VAPO-5 in comparison with literature results for different VO^{2+} systems. The parameters are obtained from the simulation of the HYSCORE spectra reported in Figures 2 and 3. Hyperfine couplings are given in MHz, the Euler angles are given in degrees.

Sample	^{31}P					^{27}Al					^{1}H					Ref
	a_{iso}	T_1	T_2	T_3	$\alpha\beta\gamma$	a_{iso}	T_1	T_2	T_3	$\alpha\beta\gamma$	a_{iso}	T_1	T_2	T_3	$\alpha\beta\gamma$	
VAPO-5	P(1) +18±1.5 P(2) +6.7±0.5 P(3) +2.0±0.5	-3.0±0.5 -1.7±0.5 -0.8±0.5	-4.0±0.5 -2.7±0.5 -0.8±0.5	+7.0±0.5 +4.3±0.5 +1.6±0.5	0,80±10,0 80±10,80±10,0 0,80±15,0	Al(1) +4.5±0.5 Al(2) +2±0.3	-2.5±0.30 -1±0.2	-2.5±0.30 -1±0.2	+5.0±0.5 +2±0.40	0,90±10,0 0,90±10,0	+4.0±1.2	-4.7±0.6	-4.7±0.6	+9.2±1.2	0,80±10,0	This work
VAPO-5	P |6|	|2.1|	|2.1|	|4.2|		Al |2|	|0.9|	|0.9|	|1.8|		+4	-4.8	-4.8	+9.6		45
VO^{2+} in bone samples	P(1) |14.25| P(2) |9.19| P(3) |3.78|	|1.87| |1.47| |1.39|	|1.87| |1.47| |1.39|	|3.74| |2.94| |2.78|												70
VO^{2+} Triphosphate	P(1) |15| P(2) |9| P(3) |1|															68
VO^{2+}-ATP	P(1) |14.8| P(2) |9.1|															65
$[VO(ADP)_2]^-$	|18.54|															66

An important feature of the X-band HYSCORE spectra (Figure 2(a)) is in fact the presence of a pronounced ridge in the (+,+) quadrant, centered at the ^{1}H Larmor frequency with a maximum width of about 13 MHz. The proton ridge is shown in Figure 3(b) along with the corresponding computer simulation (red line). The simulation of the spectrum shows that the broad proton ridge can be reproduced assuming the interaction of the unpaired electron with a single type of hydrogen nuclei. In the simulation the contribution of remote protons was added to reproduce the whole elongated ridge. The hyperfine coupling constants deduced from the simulation are reported in Table 2. Considerations based on quantum chemical calculations (*vide infra*) [lxxi] and single crystal ENDOR [lxxii] data for $[VO(H_2O)_5]^{2+}$ indicate that the parallel principal proton hyperfine value is large and positive. Following these guidelines the isotropic and dipolar components of the A^H matrix can be obtained corresponding to $a_{iso} = 4.0 \pm 1.2$ MHz and $T = 4.7 \pm 0.6$ MHz. Considering a purely dipolar interaction the V-H distance can be estimated to be 0.26 ± 0.01 nm from the following equation:

$$T = \frac{\mu_0}{4\pi} g_e g_n \beta_e \beta_n \frac{1}{r^3} \qquad (1)$$

with r being the distance between the unpaired electron localized in the V d orbitals and the ^{1}H nucleus. Importantly the same ridge extension was observed in the case of the dehydrated sample (comparison between the experimental proton ridges in the two cases is shown as Supporting Information) or the H_2 reduced sample thus excluding that the signal arises from merely coordinated water molecules, even though the hyperfine coupling constants lie in the range typical for equatorially coordinated water molecules in vanadyl systems.[lxxiii]
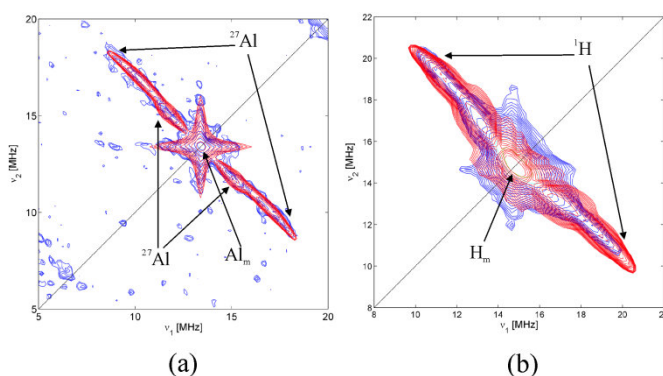

(a)   (b)

Figure 3. Experimental (blue) and simulated (red) X-band (a) and Q-band (b) HYSCORE spectra of VAPO-5. a) Q-band ^{27}Al HYSCORE spectrum recorded at $B_0 = 1210.3$ mT and T = 40K. Spectra recorded with two τ values (120, 144 ns) are summed together after Fourier transform; b) X-band ^{1}H HYSCORE spectrum recorded at $B_0 = 348.8$ mT and T = 20K. Three spectra recorded with three τ values (96, 136 and 250 ns) are summed together after Fourier transform. The spin-Hamiltonian parameters employed for the simulations are listed in Table 2. The contribution of remote Al and H nuclei is added in both cases in the simulations.

The presence of the strongly bound proton can be rationalized by a structural model of VO^{2+} replacing framework Al^{3+} ions; the charge imbalance induced by this isomorphous substitution requires a compensating positive charge to maintain the electro-neutrality of the system.

In summary, the detection of a strongly bound proton (not ascribable to merely coordinated water molecules) and the observation of the (relatively) large ^{31}P *hfi* couplings strongly points to the presence of VO^{2+} groups substituting for framework Al^{3+} ions. On the other hand the observation of the ^{27}Al couplings clearly calls for the presence of V-O-Al linkages, the presence of two different situations being in accord with the two species observed in the CW-EPR spectra and with Infra-Red stretching frequencies of adsorbed CO and NO probe molecules, indicating the presence of two VO^{2+} groups with different local environment.[35]

3.3 DFT modelling.

In order to validate the interpretation of the EPR results and translate the spin Hamiltonian parameters obtained from the EPR experiments into a microscopic description of the samples investigated, DFT calculations have been performed. Two models have been considered based on the experimental findings discussed above, which are illustrated in Figure 4 and consist of a VO^{2+} group replacing for an Al^{3+} framework ion, charge balanced by a Brönsted acid proton on a neighbouring oxygen (VO_{Al}, Figure 4a), and an extra-framework VO^{2+} group, docked in the centre of a 6 membered ring of the AFI structure (VO_{EF}, Figure 4b) where it has three P and three Al next-nearest neighbor ions. Both situations have been previously suggested in the literature 20,44,[lxxiv,lxxv]. A thorough computational analysis of the different possible V incorporation modes in the AlPO-5 structure and their relative energetics will be the object of a future work.
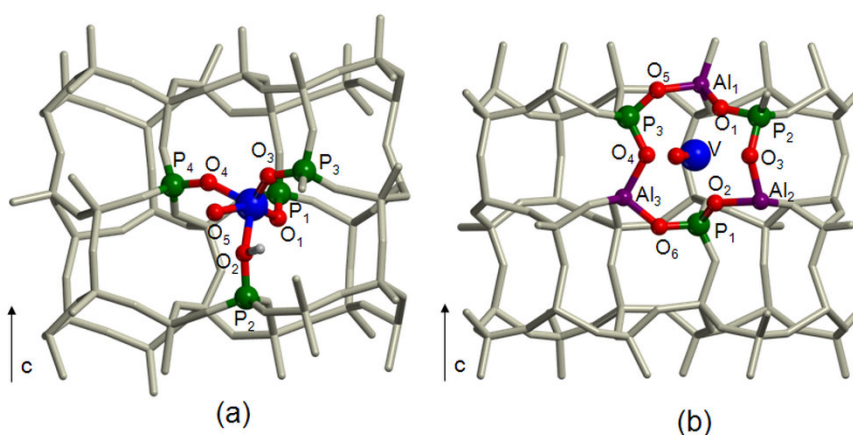

Figure 4 DFT optimized structures of monomeric vanadium centers. a) VO^{2+} substituted at a framework Al^{3+} site; b) extra-framework vanadyl group in the center of a 6-membered AlPO ring

The computed **g** and *hfi* tensors obtained for the two models are reported in Table 3. The calculated **g** factors reproduce with sufficient accuracy both the absolute values of the **g** factors and the small variations observed between the two species observed experimentally. The ^{51}V computed hyperfine parameters too are in line with the experimental findings, even though the Fermi contact term (a_{iso}) is systematically underestimated, in particular at the B3LYP level of calculation. This is a known effect related to difficult evaluation of the spin polarization at the nuclear position, where it is a small fraction of the total core electron density, in particular for heavy nuclei. Even small variations of basis set and DFT functional employed in the calculations cause large variations of the calculated a_{iso}, as shown in Table 3 when comparing B3LYP and BHandHLYP results. The dipolar term instead, is much more sensitive to the structural rather than computational details [59] and is a much more faithful reporter of the equilibrium structure around the open-shell V^{4+} ion

	g_1	g_2	g_3		a_{iso}^{B3HLY}	$a_{iso}^{BHandHLYP}$	T_1	T_2	T_3
				^{51}V	-105.3	-167.0	+82.76	+113.80	-196.56
				^{31}P1	+7.3	+3.3	-1.86	-2.33	+4.19
				^{31}P2	+1.9	+1.7	-0.84	-1.10	+1.94
VO$_{Al}$	1.9860	1.9809	1.9335	^{31}P3	+21.0	+15.4	-2.30	-2.51	+4.81
				^{31}P4	+22.1	+17.5	-2.48	-3.45	+5.93
				^{1}H	+0.16	+0.67	-3.82	-4.04	+7.86
				^{51}V	-168.6	-259.8	+94.86	+101.24	-196.10
				^{31}P1	+20.0	+15.6	-1.79	-2.84	+4.63
				^{31}P2	+18.9	+14.6	-2.15	-2.45	+4.60
VO$_{EF}$	1.9876	1.9867	1.9340	^{31}P3	+12.9	+9.83	-1.77	-2.40	+4.17
				^{27}Al1	+3.5	+2.6	-0.51	-0.91	+1.42
				^{27}Al2	+4.7	+3.7	-0.87	-1.01	+1.87
				^{27}Al3	+2.6	+1.9	-0.50	-0.70	+1.20

Table 3. DFT computed **g** and ^{51}V *hfi* tensor elements (in MHz) relative to the model structures illustrated in Figure 4. The numbering of the atoms is given in Figure 4.

The ^{31}P *hfi* couplings computed for the framework and extraframework models of the VO^{2+} group are both in reasonable agreement with the experimental data. The ^{31}P a_{iso} coupling is found to vary significantly depending on the V-O-P angles and distances, similarly to what reported by Arieli et al.[47] in the case of Mn-O-P linkages in MnAPO systems. The subtle interplay between bond length and bond angles of the V-O-P units, leads to a distribution of values, which is representative of the experimental findings, demonstrating that the different couplings observed in the ^{31}P HYSCORE experiments originate from the interaction of the unpaired electron mainly localized in the V d orbitals, with different O-P units of the framework. In the case of the VO$_{Al}$ model, the computed ^{31}P a_{iso} couplings show a large distribution, ranging from 1.7 MHz to 17.5 MHz, with two P nuclei

(P2 and P3) giving very similar values. In the case of the extraframework species (VO$_{EF}$) the ^{31}P *hfi* couplings range between 9.8 MHz and 15.6 MHz, compatible with the largest couplings observed experimentally. The experimental HYSCORE spectra could be simulated considering three distinct ^{31}P nuclei, however the similarity of some of the computed values suggests that the presence of overlapping (unresolved) signals may indeed be present. The ^{1}H computed *hfi* values for the VO$_{Al}$ species are also in reasonable agreement with the experimental values, in particular for the dipolar term, while the Fermi contact term is underestimated – for the same reason already discussed for ^{51}V.

The computed ^{27}Al a_{iso} couplings for the VO$_{EF}$ structure, illustrated in Figure 4b, reflect the trend observed for the ^{31}P couplings, on a smaller scale, consistent with the smaller a_0 value computed for unit occupancy of the ^{27}Al 3s orbital with respect to the ^{31}P 3s orbital.[69] The computed values range between 1.9 MHz and 3.7 MHz which compare relatively well with the experimentally deduced values of 2.0 MHz and 4.5 MHz. In the case of the largest coupling the computed anisotropic contribution is underestimated with respect to the experimental result. Apart from this small discrepancy, the overall computed properties for the two models can be taken as a satisfactory reproduction of the experimental results, and hence the two structural models chosen for the vanadyl ion are representative of the real VAPO catalyst.

Summarizing, the computed EPR properties for the two models reported in Figure 4, account fairly well for the experimentally observed data, indicating that framework substituted and extra-framework VO^{2+} species can be taken as representative of the two EPR active species observed in the experiments. The presence of two VO groups is in agreement with UV-Vis spectra, which are characterized by a broad and unresolved absorption in the typical region of VO^{2+} ions (see Ref. 35 for a more detailed discussion). The isomorphous replacement of Al^{3+} framework sites is consistent with the measured sample formula Al$_{16.1}$P$_{16.9}$V$_{0.2}$O$_{66.3}$, showing a slightly lower amount of Al framework atoms with respect to P. Moreover, infrared spectra of probe molecules adsorbed on the same sample showed the presence of two distinct vanadyl-like sites,[35] consistent with the presence of framework and extra framework vanadyl species.

Conclusions.

The relevant findings obtained from the present study of V doped AlPO-5 materials can be summarized as follows:

a)   CW EPR spectra indicate the presence of two slightly different species amenable to highly dispersed V^{4+} ions. The intensity ratio of the two species is approximately 1:0.7 and the spin

19

Hamiltonian parameters are in agreement with values expected for VO^{2+} species. The spin Hamiltonian parameters remain virtually unchanged upon calcination and dehydration at 423 K of the sample.

b)   HYSCORE spectra recorded on both as received, calcined/de-hydrated and reduced samples reveal the presence of distinct ^{31}P and ^{27}Al cross peaks associated to relatively large hyperfine interactions dominated by the Fermi contact term, implying spin density transfers ranging in the interval 0.2% - 0.02%, consistent with V-O-P and V-O-Al structural entities.

c)   A ^1H signal is observed whose features agree with the presence of one equatorial proton in the first coordination shell of the VO^{2+} species. Importantly the ^1H ridge remains almost unaltered upon dehydration of the sample excluding the possibility to assign it to coordinating water molecules.

The data can be interpreted in term of two distinct species amenable to two VO^{2+} entities with local environment constituted by ^{31}P, ^{27}Al and ^1H nuclei. Two possible models have then been considered in order to account for the experimental results, consisting of VO^{2+} species isomorphously substituted at Al^{3+} sites and extra-framework VO^{2+} ions grafted on the surface of the solid. DFT computed EPR data for the two models reproduce well the experimental observables indicating that the experimental results can be explained considering that a fraction of V in the form of VO groups, isomorphously replaces Al^{3+} framework sites, while another fraction, is present as extraframework VO species. It is important to note that the presence of extra-framework sites is the direct consequence of the complex chemistry of vanadium with respect to other transition metal ions such as titanium, for which direct evidence for isomorphous substitution at Al^{3+} and P^{5+} sites has been obtained by means of advanced EPR experiments [24] and recently corroborated by X-ray absorption and emission studies.[lxxvi]

In this work we concentrated exclusively on the EPR properties of V^{4+} species and we cannot exclude the presence of (EPR silent) V^{5+}, isomorphously substituting for framework P^{5+}. If present, these centers are not easily reducible, which seems to be a distinctive feature of transition metal ions incorporated at P^{5+} sites of AlPO materials.

Supporting Information Available

XRD patterns of VAPO-5 sample after calcination and repeated oxidation/reduction cycles, CW-EPR and HYSCORE experiment on reduced VAPO samples, HYSCORE simulations at different magnetic field settings, atomic coordinates of the two optimized V clusters. This information is available free of charge via the Internet at http://pubs.acs.org

References

[1] Thomas, J. M. The Concept, Reality and Utility of Single-Site Heterogeneous Catalysts (SSHCs) *Phys. Chem. Chem. Phys.* **2014**, *16*, 7647-7661.

[2] Martínez, C.; Corma, A. Inorganic Molecular Sieves: Preparation, Modification and Industrial Application in Catalytic Processes *Coord. Chem. Rev*. **2011**, *255*, 1558-1580.

[3] Gómez-Hortigüela, L; Corà, F.; Catlow, C. R. A. Aerobic Oxidation of Hydrocarbons Catalyzed by Mn-Doped Nanoporous Aluminophosphates(I): Preactivation of the Mn Sites *ACS Catal.*, **2011**, *1*, 18-28.

[4] Pastore, H. O.; Coluccia, S.; Marchese, L. Porous Aluminophosphates: From Molecular Sieves to Designed Acid Catalysts *Ann. Rev. Mater. Res.* **2005**, *35*, 351-395.

[5] Raja R.; Sankar G.; Thomas J.M. Bifunctional Molecular Sieve Catalysts for the Benign Ammoximation of Cyclohexanone: One-Step, Solvent-Free Production of Oxime and ε-Caprolactam with a Mixture of Air and Ammonia *J. Am. Chem. Soc*. **2001**, *123*, 8153-8154.

[6] Thomas, J. M. Design, Synthesis, and In Situ Characterization of New Solid Catalysts *Angew. Chem., Int. Ed*. **1999**, *38*, 3589-3628.

[7] Raja, R.; Potter, M. E.; Newland, S. H. Predictive Design of Engineered Multifunctional Solid Catalysts *Chem. Commun.* **2014**, *50*, 5940-5957.

[8] Raja, R.; Thomas, J.M.; Xu, M.; Harris, K. D. M.; Greenhill-Hooper, M.; Quill, K. Highly Efficient One-Step Conversion Of Cyclohexane to Adipic Acid Using Single-Site Heterogeneous Catalysts *Chem. Commun*. **2006**, 448-450.

[9] Modén B.; Zhan B.Z.; Dakka J.; Santiesteban J.G.; Iglesia E. Reactant Selectivity and Regiospecificity in the Catalytic Oxidation of Alkanes on Metal-Substituted Aluminophosphates *J. Phys. Chem. C* **2007**, *111*, 1402-1411.

[10] Saadoune, I.; Corà, F.; Alfredsson, M.; Catlow, C.R.A. Computational Study of the Structural and Electronic Properties of Dopant Ions in Microporous AlPOs. 2. Redox Catalytic Activity of Trivalent Transition Metal Ions *J. Phys. Chem. B* **2003**, *107*, 3012-3018.

[11] Arends, I. W. C. E.; Sheldon, R. A.; Wallau, M.; Schuchardt, U. Oxidative Transformations of Organic Compounds Mediated by Redox Molecular Sieves *Angew. Chem., Int. Ed. Engl.* **1997**, *36*, 1144-1163.

[12] Thomas, J. M.; Raja, R.; Sankar, G.; Bell, R. Molecular-Sieve Catalysts for the Selective Oxidation of Linear Alkanes by Molecular Oxygen *Nature* **1999**, *298*, 227-230.

[13] Hartmann, M., Kevan, L., Transition-Metal Ions in Aluminophosphate and Silicoaluminophosphate Molecular Sieves: Location, Interaction with Adsorbates and Catalytic Properties *Chem. Rev*. **1999,** *99*, 635-664.

[14] Thomson, S.; Luca, V.; Howe, R. Framework Co(II) in CoAPO-5 *Phys. Chem. Chem. Phys*. **1999,** *1*, 615-619.

[15] Barrett, P.A.; Sankar, G.; Catlow, C.R.A.; Thomas, J.M. Investigation of the Structural Stability of Cobalt-Containing AlPO-44 Microporous Materials *J. Phys. Chem. Solids* **1995**, *56*, 1395-1405.

[16] Modén, B.; Oliviero, L.; Dakka, J.; Santiesteban, J.G.; Iglesia, E. Structural and Functional Characterization of Redox Mn and Co Sites in AlPO Materials and Their Role in Alkane Oxidation Catalysis *J. Phys. Chem.* B **2004**, *108*, 5552-5563.

[17] Marchese, L.; Chen, J.S.; Thomas, J.M.; Coluccia, S.; Zecchina, A. Bronsted, Lewis, and Redox Centers on CoAPO-18 Catalysts. 1. Vibrational Modes of Adsorbed Water *J. Phys. Chem*. **1994**, *98*, 13350-13356.

[18] Saadoune, I.; Corà, F.; Catlow, C.R.A. Computational Study of the Structural and Electronic Properties of Dopant Ions in Microporous AlPOs. 1. Acid Catalytic Activity of Divalent Metal Ions *J. Phys. Chem. B* **2003**, *107*, 3003-3011.

[19] Prakash, A. M.; Kevan, L. Location and Adsorbate Interactions of Vanadium in VAPO-5 Molecular Sieve Studied by Electron Spin Resonance and Electron Spin Echo Modulation Spectroscopies *J. Phys. Chem. B*, **1999**, *103*, 2214-2222.

[20] Weckhuysen, B. M.; Vannijvel, I. P.; Schoonheydt, R. A. Chemistry and Spectroscopy of Vanadium in VAPO-5 Molecular Sieves *Zeolites*, **1995**, *15*, 482-489.

[21] Zahedi-Niaki, M. H.; Zaidi, S. M. J.; Kaliaguine, S. Comparative Study of Vanadium Aluminophosphate Molecular Sieves VAPO-5, -11, -17 and -31 *Appl. Catal. A-Gen.* **2000**, *196*, 9-24.

[22] Fan, W.B.; Fan, B.B.; Song, M.G.; Chen, T.H.; Li, R.F.; Dou, T.; Tatsumi, T.; Weckhuysen, B.M. Synthesis, Characterization and Catalysis of (Co,V)-, (Co,Cr)- and (Cr,V)-APO-5 Molecular Sieves *Microporous Mesoporous Mater.* **2006**, *94*, 348-357.

[23] Venkatathri, N.; Shetty, V. N. Synthesis and Characterization of TAPO-31 Molecular Sieves Using Tripropylamine Template *Catal. Commun.*, **2006**, *7*, 1015-1021.

[24] Maurelli, S.; Muthusamy, V.; Chiesa, M.; Berlier, G.; Van Doorslaer, S. Elucidating the Nature and Reactivity of Ti Ions Incorporated in the Framework of AlPO-5 Molecular Sieves. New Evidence from ^{31}P HYSCORE Spectroscopy *J. Am. Chem. Soc.* **2011**, *133*, 7340-7343.

25 Maurelli, S.; Vishnuvarthan, M.; Berlier, G.; Chiesa, M. NH$_3$ and O$_2$ Interaction with Tetrahedral Ti^{3+} Ions Isomorphously Substituted in the Framework of TiAlPO-5. A Combined Pulse EPR, Pulse ENDOR, UV-Vis and FT-IR Study *Phys. Chem. Chem. Phys.* **2012**, *14*, 987-995.

26 Concepción, P.; López Nieto, J. M.; Mifsud, A.; Pérez-Pariente, J. Synthesis, Characterization and Catalytic Properties of Microporous MgVAPO-5 *Appl. Catal. A* **1997**, *151*, 373-392.

27 Concepción, P.; Corma, P.; López Nieto, J. M.; Pérez-Pariente, J. Selective Oxidation of Hydrocarbons on V-and/or Co-Containing Aluminophosphate (MeAPO-5) Using Molecular Oxygen *Appl. Catal. A* **1996,** *143*, 17-28.

28 Itoh, T.; Jitsukawa, K.; Kaneda, K.; Teranishi, S. Vanadium-Catalyzed Epoxidation of Cyclic Allylic Alcohols. Stereoselectivity and Stereocontrol Mechanism *J. Am. Chem. Soc.* **1979**, *101*, 159-169.

29 Sharpless, K. B.; Michaelson, R. C. High Stereo- and Regioselectivities in the Transition Metal Catalyzed Epoxidations of Olefinic Alcohols by Tert-Butyl Hydroperoxide *J. Am. Chem. Soc.* **1973**, *95*, 6136-6137.

30 Mimoun, H.; Mignard, M.; Brechot, P.; Saussine, L. Selective Epoxidation of Olefins by Oxo[N-(2-oxidophenyl)salicylidenaminato]Vanadium(V) Alkylperoxides. On the Mechanism of the Halcon Epoxidation Process *J. Am. Chem. Soc.* **1986**, *108*, 3711-3718.

31 Concepción P.; López Nieto J. M.; Pérez-Pariente J. The Selective Oxidative Dehydrogenation of Propane on Vanadium Aluminophosphate Catalysts *Catal. Lett.* **1993**, *13*, 333-337.

32 Miyamoto, A.; Iwamoto, Y.; Matsuda, Y.; Inui, T. Selective Ammoxidation of Propane on Vanadoaluminophosphate Catalysts *Stud. Surf. Sci. Catal.* **1990**, *49*, 1233-1242.

33 Maurelli, S.; Chiesa, M.; Giamello, E.; Leithall, R. M.; Raja, R. A HYSCORE Investigation of Bimetallic Titanium–Vanadium Microporous Catalysts: Elucidating the Nature of the Active Sites *Chem. Commun.* **2012**, *48*, 8700.

34 Leithall, R.; Shetti, V.; Maurelli, S.; Chiesa, M.; Gianotti, E.; Raja, R. Toward Understanding the Catalytic Synergy in the Design of Bimetallic Molecular Sieves for Selective Aerobic Oxidations *J. Am. Chem. Soc.* **2013**, *135*, 2915-2918.

35 Vishnuvarthan, M.; Paterson, A. J.; Raja, R.; Piovano, A.; Bonino, F.; Gianotti, E.; Berlier, G. Spectroscopic Investigation into the Nature of the Active Sites for Epoxidation Reactions Using Vanadium-Based Aluminophosphate Catalysts *Microporous Mesoporous Mater.* **2011**, *138*, 167-175.

36 Cheng, H.Y.; Yang, E.; Lai, C.J.; Chao, K.J.; Wei, A.C.; Lee, J.F. Density Functional Theory Calculation and X-ray Absorption Spectroscopy Studies of Structure of Vanadium-Containing Aluminophosphate VAPO-5 *J. Phys. Chem. B* **2000**, *104*, 4195-4203.

37 Frunza, L.; Van Der Voort, P.; Vansant, E. F.; Schoonheydt, R. A.; Weckhuysen, B. M. On the Synthesis of Vanadium Containing Molecular Sieves by Experimental Design from a VOSO$_4$·5H$_2$O·Al(iPrO)$_3$·Pr$_2$NH·H$_2$O Gel: Occurrence of VAPO-41 as a Secondary Structure in the Synthesis of VAPO-11 *Microporous Mesoporous Mater.* **2000**, *39*, 493-507.

38 Wei, A.; Chao, K. J. Structural Characterization of Metal Ions Incorporated in Molecular Sieve Frameworks *Chinese. Chem. Soc.* **2000,** *47*, 33-40.

39 Weckhuysen, B. M.; Rao, R. R.; Martens, J. A.; Schoonheydt, R. A. Transition Metal Ions in Microporous Crystalline Aluminophosphates: Isomorphous Substitution *Eur. J. Inorg. Chem.* **1999**, 565-577.

40 Dinse, A.; Wolfram, T.; Carrero, C.; Schlögl, R.; Schomäcker, R.; Dinse, K.-P. Exploring the Structure of Paramagnetic Centers in SBA-15 Supported Vanadia Catalysts with Pulsed One- and Two-Dimensional Electron Paramagnetic Resonance (EPR) and Electron Nuclear Double Resonance (ENDOR) *J. Phys. Chem. C* **2013**, *117*, 16921-16932.

41 Woodworth, J.; Bowman, M. K.; Larsen, S. C. Two-Dimensional Pulsed EPR Studies of Vanadium-Exchanged ZSM-5 *J. Phys. Chem. B* **2004**, *108*, 16128-16134.

42 Chiesa, M.; Meynen, V.; Doorslaer, S. V.; Cool, P.; Vansant, E. F. Vanadium Silicalite-1 Nanoparticles Deposition onto the Mesoporous Walls of SBA-15. Mechanistic Insights from a Combined EPR and Raman Study *J. Am. Chem. Soc.* **2006**, *128*, 8955-8963.

43 Nagarajan, V.; Müller, B.; Storcheva, O.; Köhler, K.; Pöppl, A. Structure and Bonding of [V(IV)O(acac)$_2$] on the Surface of AlF$_3$ as Studied by Pulsed Electron Nuclear Double Resonance and Hyperfine Sublevel Correlation Spectroscopy *Phys. Chem. Chem. Phys.* **2009**, *11*, 6849-6854.

44 Pöppl, A.; Manikandan, P.; Köhler, K.; Maas, P.; Strauch, P.; Böttcher, R.; Goldfarb, D. Elucidation of Structure and Location of V(IV) Ions in Heteropolyacid Catalysts H$_4$PVMo$_{11}$O$_{40}$ as Studied by Hyperfine Sublevel Correlation Spectroscopy and Pulsed Electron Nuclear Double Resonance at W- and X- Band Frequencies *J. Am. Chem. Soc.* **2001**, 123, 4577-4584.

45 Nagarajan, V.; Rings, D.; Moschkowitz, L.; Hartmann, M.; Pöppl, A. Location of Vanadium(IV) in VAPO-5 as Studied by Hyperfine Sublevel Correlation Spectroscopy *Chem. Lett.* **2005**, *34*, 1614-1615.

46 Arieli, D.; Vaughan, D. E. W.; Strohmaier, K. G.; Goldfarb, D. High Field ^{31}P ENDOR of MnAlPO$_4$-20: Direct Evidence for Framework Substitution *J. Am. Chem. Soc.* **1999**, 121, 6028-6032.

22

47   Arieli, D.; Delabie, A.; Groothaert, M.; Pierloot, K.; Goldfarb, D. The Process of Mn(II) Incorporation into Aluminophosphate Zeotypes Through High-Field ENDOR Spectroscopy and DFT Calculations *J. Phys. Chem. B* **2002**, *106*, 9086-9097.

48   Höfer, P.; Grupp, A.; Nebenfür, H.; Mehring, M. Hyperfine Sublevel Correlation (HYSCORE) Spectroscopy: a 2D ESR Investigation of the Squaric Acid Radical *Chem. Phys. Lett.* **1986**, *132*, 279-282.

49   Stoll, S.; Schweiger, A. EasySpin, a Comprehensive Software Package for Spectral Simulation and Analysis in EPR *J. Magn. Reson.* **2006**, *178*, 42-55.

50   Corà, F.; Alfredsson, M.; Barker, C. M.; Bell, R. G.; Foster, M. D.; Saadoune, I.; Simperler, A.; Catlow, C. R. A. Modeling the Framework Stability and Catalytic Activity of Pure and Transition Metal-Doped Zeotypes *J. Solid State Chem.* **2003**, *176*, 496-529.

51   Dovesi, R.; Orlando, R.; Civalleri, B.; Roetti, C.; Saunders, V. R.; Zicovich-Wilson, C. M. CRYSTAL: a Computational Tool for the Ab Initio Study of the Electronic Properties of Crystals *Z. Kristallogr.* **2005**, *220*, 571-573.

52   Dovesi, R.; Saunders, V. R.; Roetti, C.; Orlando, R.; Zicovich-Wilson, C. M.; Pascale, F.; Civalleri, B.; Doll, K.; Harrison, N. M.; Bush, I. J.; D'Arco, P.; Llunell M. CRYSTAL09 User's Manual; University of Torino: Torino, **2009**.

53   Becke, A. D. Density-Functional Thermochemistry. 3. The Role of Exact Exchange *J. Chem. Phys.* **1993**, *98*, 5648-5652.

54   Lee, C.; Yang, W.; Parr, R. G. Development of the Colle-Salvetti Correlation-Energy Formula into a Functional of the Electron Density *Phys. Rev. B* **1988**, *37*, 785-789.

55   http://www.crystal.unito.it/basis-sets.php

56   Neese, F. The ORCA program system *Wiley Interdiscip. Rev.: Comput. Mol. Sci.* **2012**, *2*, 73-78.

57   Sandhoefer, B.; Neese, F. One-electron Contributions to the **g**-tensor for Second-Order Douglas-Kroll-Hess Theory *J. Chem. Phys.* **2012**, *137*, 094102-1 - 094102-15.

58   Schafer, A.; Huber, C.; Ahlrichs, R. Fully Optimized Contracted Gaussian-Basis Sets of Triple Zeta Valence Quality for Aroms Li to Kr *J. Chem. Phys.* **1994**, *100*, 5829-5835.

59   Saladino, A. C.; Larsen, S. C. Density Functional Theory Calculations of the Electron Paramagnetic Resonance Parameters for VO^{2+} Complexes *J. Phys. Chem. A* **2003**, *107*, 1872-1878.

60   Becke, A. D. A New Mixing of Hartree-Fock and Local Density-Functional Theories *J. Chem. Phys.* **1993**, *98*, 1372-1377.

61   Selbin, J. The Chemistry of Oxovanadium(IV) *Chem. Rev.* **1965**, *65*, 153-175.

62   Lohse, U.; Brückner, A.; Kintscher, K.; Parlitz, B.; Schreier, E. Synthesis and Characterization of VAPSO-44 and VAPSO-5 *J. Chem. Soc., Faraday Trans.* **1995**, *91*, 1173-1178.

63   Jakes, P.; Eichel, R.-A. Characterization of Tetravalent Vanadium Functional Centres in Metal Oxides Derived from a Spin-Hamiltonian Analysis. *Mol. Phys.* **2012**, *110*, 277−282.

64   Nayarany, M.; Kevan, L. Reinterpretation of the State of Paramagnetic Vanadium Species in Alluminophosphates. *J. Phys. C: Solid State Phys.* **1983**, *16*, L863−L866.

65   Buy, C.; Matsui, T.; Andrianambinintsoa, S.; Sigalat, C.; Girault, G.; Zimmermann, J.-L. Binding Sites for Mg(II) in H^+-ATPase from Bacillus PS3 and in the $\alpha_3\beta_3\gamma$ Subcomplex Studied by One-Dimensional ESEEM and Two-Dimensional HYSCORE Spectroscopy of Oxovanadium(IV) Complexes: A Possible Role for β-His-324 *Biochemistry* **1996**, *35*, 14281-14293.

66   Mustafi, D.; Telser, J.; Makinen, M. W. Molecular Geometry of Vanadyl-Adenine Nucleotide Complexes Determined by EPR, ENDOR, and Molecular Modeling *J. Am. Chem. Soc.* **1992**, *114*, 6219-6226.

67   Petersen, J.; Fisher, K.; Lowe, D. J. Structural Basis for VO^{2+} Inhibition of Nitrogenase Activity (A): ^{31}P and ^{23}Na Interactions with the Metal at the Nucleotide Binding Site of the Nitrogenase Fe Protein Identified by ENDOR Spectroscopy *J. Biol. Inorg. Chem.* **2008**, *13*, 623-635.

68   Dikanov, S. A.; Liboiron, B. D.; Orvig, C. Two-Dimensional (2D) Pulsed Electron Paramagnetic Resonance Study of VO^{2+}−Triphosphate Interactions: Evidence for Tridentate Triphosphate Coordination, and Relevance To Bone Uptake and Insulin Enhancement by Vanadium Pharmaceuticals *J. Am. Chem. Soc.* **2002**, *124*, 2969-2978.

69   Fitzpatrick, J. A. J.; Manby, F. R.; Western, C. M. The Interpretation of Molecular Magnetic Hyperfine Interactions *J. Chem. Phys.* **2005**, *122*, 084312-1 - 084312-12.

70   Dikanov, S. A.; Liboiron, B. D.; Thompson, K. H.; Vera, E.; Yuen, V. G.; McNeill, J. H.; Orvig, C. In Vivo Electron Spin−Echo Envelope Modulation (ESEEM) Spectroscopy: First Observation of Vanadyl Coordination to Phosphate in Bone *J. Am. Chem. Soc.* **1999**, *121*, 11004-11005.

lxxi   Larsen, S. C. DFT Calculations of Proton Hyperfine Coupling Constants for $[VO(H_2O)_5]^{2+}$: Comparison with Proton ENDOR Data *J. Phys. Chem. A* **2001**, *105*, 8333-8338.

lxxii   Atherton, N. M.; Shackleton, J. F. Proton ENDOR of $VO(H_2O)_5^{2+}$ in $Mg(NH_4)_2(SO_4)_2)_2 6H_2O$ *Mol. Phys.* **1980**, *39*, 1471-1485.

23

lxxiii Mustafi, D.; Makinen, M. W. ENDOR-Determined Solvation Structure of vanadyl(2+) in Frozen Solutions *Inorg. Chem.* **1988**, *27*, 3360-3368.

lxxiv Rigutto, M. S.; van Bekkum, H. J. Vanadium Site in VAPO-5: Characterization and Catalytic Properties in Liquid-Phase Alkene Epoxidation and Benzylic Oxidation *J. Mol. Catal*. **1993**, *81*, 77-98.

lxxv Lohse, U.; Buckner, A.; Kintscher, K.; Parlitz, B.; Schreier, E. Synthesis and Characterization of VAPSO-44 and VAPSO-5 *J. Chem. Soc*. *Faraday*. *Trans*. **1995**, *91*, 1173-1178.

lxxvi Gallo, E.; Piovano, A.; Marini, C.; Mathon, O.; Pascarelli, S.; Glatzel, P.; Lamberti, C.; Berlier, G. Architecture of the Ti(IV) Sites in TiAlPO-5 Determined Using Ti K-Edge X-ray Absorption and X-ray Emission Spectroscopies *J. Phys. Chem. C.* **2014**, *118*, 11745–11751.